

http://www.doi.org/10.62341/AKBM2379

Received	2025/10/28	تم استلام الورقة العلمية في
Accepted	2025/11/18	تم قبول الورقة العلمية في
Published	2025/11/19	تم نشر الورقة العلمية في

Thermo-mechanics of Eco-concrete Beams Reinforced with Waste Pottery.

Abdelmoutalib BENFRID 1, 2, Krzysztof MURAWSKI 3

¹ Doctor in Public Works, graduated from Djillali Liabès University in Sidi Bel Abbès, Algeria.

²Libyan Society for Research and Scientific Studies. - Libya

³Dr. inż. (PhD), Poland, Former Assistant Professor at the Jacob of Paradies University of Gorzów Wlkp. and at the University of Life Sciences in Poznan, Assistant at the University of Technology of Zielona Góra.

Corresponding Author Email: benfridabdelmoutalib2050@gmail.com

Abstract:

Eco-concretes are essential to integrate into civil engineering for environmental reasons. Beams, which are load-bearing elements of civil engineering structures, are subjected to mechanical and thermal loads. In this study, mechanical and thermal deformations are analyzed on beams reinforced with Pottery powder at different concentrations. The thermoelastic properties of the eco-concrete are obtained using the Mori-Tanaka model. The studied deformation takes into account the shear effect introduced by a mathematical function. The principle of virtual work is used to establish the equilibrium equations, and then Navier's solutions are applied to solve the mathematical problem of thermomechanical bending. It is found that as the concentration of Pottery powder increases, the mechanical deformation decreases. Eco-concretes also show strong resistance to thermomechanical behavior and the influence of temperature. Furthermore, it is shown that it is possible to incorporate up to 30% of aluminosilicate waste in the form of Pottery powder.

Keywords: Eco-concretes- Mori-Tanaka model- thermal deflection- mechanical deflection- Pottery powder.



http://www.doi.org/10.62341/AKBM2379

الميكانيكا الحرارية للعوارض الخرسانية البيئية المدعمة بنفايات الفخار. بن فريد عبد المطلب 1,2 كرزيستوف موراوسكي 3

. دكتوراه في الأشغال العمومية ، تخرج من جامعة جلالي ليبس في سيدي بالعباس، الجزائر 1 دكتوراه في الأشغال العمومية اللبيبة للبحوث والدراسات العلمية. ليبيا

 3 د. إنز. (دكتوراه)، بولندا، أستاذ مساعد سابق في جامعة جاكوب باراديس في غورزوف فولكب. وفي جامعة علوم الحياة في بوزنان، مساعد في جامعة زيلونا غورا للتكنولوجيا.

الملخص:

الخرسانة البيئية ضرورية للاندماج في الهندسة المدنية لأسباب بيئية. تتعرض الحزم، وهي عناصر حاملة لهياكل الهندسة المدنية، لأحمال ميكانيكية وحرارية. في هذه الدراسة، تم تحليل التشوهات الميكانيكية والحرارية على عوارض مدعمة بمسحوق الفخار بتركيزات مختلفة. يتم الحصول على الخصائص المرنة الحرارية للخرسانة البيئية باستخدام نموذج موري تاناكا. يأخذ التشوه المدروس في الاعتبار تأثير القص الذي أدخلته دالة رياضية. يستخدم مبدأ العمل الافتراضي لتحديد معادلات التوازن، ثم يتم تطبيق حلول نافييه لحل المشكلة الرياضية للانحناء الميكانيكي الحراري. وجد أنه مع زيادة تركيز مسحوق الفخار، ينخفض التشوه الميكانيكي. تظهر الخرسانة البيئية أيضا مقاومة قوية للسلوك الحراري الميكانيكي وتأثير درجة الحرارة. علاوة على ذلك، تبين أنه من الممكن دمج ما يصل إلى 30% من نفايات سيليكات الألومنيوم على شكل مسحوق فخار.

الكلمات المفتاحية: الخرسانة البيئية - نموذج موري تاناكا - الانحراف الحراري - الانحراف الميكانيكي - مسحوق الفخار

1. Introduction

Eco-concretes enhanced with silica have demonstrated substantial improvements in mechanical properties, as evidenced by several studies. F. Boukhelf et al. found that incorporating 20% to 30% glass powder increases workability and slightly enhances the strength of hardened concrete [1]. R.Z. Harrat et al. studied the effects of nano-silica on flexural beams, noting silica's tendency to agglomerate at the corners of beams, which affects performance [2]. M. Chatbi et al. focused on silica's agglomeration in concrete to better understand slab deflection [3], while A.M. Benfrid et al.



http://www.doi.org/10.62341/AKBM2379

identified that nano-glass reinforcement negatively impacts the thermal bending of eco-concrete panels [4]. S. Diene El Hannani's research highlighted the benefits of beams reinforced with nano-inclusions, which improved concrete's overall performance.[5]

A. Kecir et al. observed that nano-irons enhanced the mechanical strength of concrete but reduced its thermal resistance [6]. Further investigations by M. Chatbi et al. used the Eshelby model to understand the concrete's stiffness tensor with nano-clays [7], and R.Z. Harrat et al. applied the same model to assess the of concrete containing nano-irons, thermoelasticity improvements in mechanical performance at the expense of thermal properties [8]. A.M. Benfrid et al. found that concrete containing siliceous and alumino-silicate glass powders had low heat transfer, with varying Young's modulus depending on direction [9], and later research revealed that organic reinforcements weakened the concrete and led to poor bending performance [10]. The Mori-Tanaka model has been extensively used in the study of reinforced concrete, especially in assessing materials like nano-tungsten. A.J. Benbakhti et al. employed this model for the repair of corroded wastewater treatment plants, improving steel reinforcement properties with nano-tungsten [11]. L. Melati et al. showed that increasing nano-tungsten concentration in a two-phase medium reduced deflection in concrete beams [12]. X. Wang et al. experimentally validated the Mori-Tanaka model, demonstrating its close match with experimental results [13], while other studies confirmed its reliability in thermoelastic predictions for concrete [14][15][16][17][18][20].Beam thermoelasticity has been explored through various models, including S.M. Ghumare et al.'s study on functionally graded beams [21] and Y. Boulahbal et al.'s development of a non-linear model for hygro-thermo-mechanical analysis of beams [22]. M.F. Ertenli et al. analyzed the effects of porosity and shear on curved beam behavior under thermomechanical loading [23], and A.S. Sayyad et al. examined shell hygro-thermo-elastic properties with a shear function [24]. Further, K. Meski et al. used Reddy's theory to study functionally graded beam performance under various parameters [25], while the Mori-Tanaka model was used to analyze the thermoelasticity of concrete reinforced with glass powder and silica.[26]

The study of beam stability under axial loads has been advanced by Murawski's exploration of semi-slender steel columns under elastoplastic compression, where he compared models like



http://www.doi.org/10.62341/AKBM2379

Tetmajer-Jasiński and Johnson-Ostenfeld [30][31]. Krzysztof Murawski's work on slender columns revealed that thin columns become unstable under axial load, highlighting the importance of accurate structural modeling for these types of elements [30][31]. Charles Chinwuba Ike used the Ritz variational method to analyze the vibrations of slender beams supported by elastic foundations, highlighting its effectiveness in predicting frequencies under various boundary conditions [32]. In another study, Ike applied this method to shear-deformable material theory, revealing the potential for overestimating buckling loads in thick beams [33]. Mladenov's research focused on beam eccentricities and stress-free construction, distinguishing between strained and deformed elements under various loading conditions [34]. Doicheva further challenged assumptions on the impact of eccentric connections and off-center supports on stress-strain behavior, showing realistic results that differed 15-30% from theoretical predictions [35]. Boukhari et al. used the Mori-Tanaka model to study granite powder-reinforced concrete beams, finding that increased granite content improved mechanical properties while reducing deflection and displacement [36]. Yakro et al. also applied this model to concrete mixed with glass and brick waste, showing that waste materials improved mechanical properties but weakened thermal performance.[37]

Melati et al. proposed a refined plate theory for studying nanocomposite plate bending with a steel-nano-tungsten alloy, using the Mori-Tanaka homogenization scheme to validate elastic properties and stress-displacement responses [38]. Peker's study of a 14-story dual-system building after the 2023 Kahramanmaraş earthquakes showed that the dual shear wall-frame system performed better than surrounding buildings in terms of seismic resistance [39], while Aras et al. and Işık et al. found that even seismically compliant buildings sustained significant damage due to brick infill walls, with PRF wrapping recommended to enhance column resistance [40.[41] [

Further research on orthotropic porous materials by Furkan Can Bahadır and Ferruh Turan examined the free vibrations of cylindrical panels with orthotropic porous layers, showing that factors like porosity and geometry influence vibrational responses [42]. Demir and Turan explored the stability of laminated cylindrical panels under varying linear compression, simulating porous material behavior and its effect on buckling [43]. Krzysztof



http://www.doi.org/10.62341/AKBM2379

Murawski's study on St35 steel columns with arched flaws provided critical insights into the stability of semi-slender columns under axial compression, comparing results from finite element methods and classical theories [44]. Dao Ngoc Tien et al. applied classical and refined plate theory to derive governing equations for static SCC slabs, revealing how plate thickness affects deflection [45]. Lastly, Tuan-Anh Bui and colleagues modeled rigid pavements shaking on uneven foundations, using finite element analysis and Mindlin's plate theory to demonstrate how foundation stiffness impacts vibration modes and frequencies [46]. Ferruh Turan et al. studied thin-walled orthotropic porous I-beams under lateral loads, showing that web thickness and porosity distributions reduce critical buckling loads and improve beam stability [47]. Peng Shi et al. applied neural network models to analyze the vibration response of functionally graded sandwich plates, emphasizing the impact of the thickness ratio on system stiffness [48]. These studies highlight the essential role of the Mori-Tanaka model in understanding the thermo-mechanical behavior of composite materials, especially in eco-concrete and reinforced systems. The research also underscores significant advances in structural stability, vibration analysis, and material performance under various loading conditions.

2. Mori-Tanaka Homogenization

- Ec: The elasticity modulus of concrete .
- Ew: The elasticity modulus of Waste.
- Ehom: The homogenized elasticity modulus.
- Gc: The shear modulus of Concrete.
- Gw: The shear modulus of waste. -Ghom: The homogenized shear modulus.
- K_c: The bulk modulus of Concrete.
- K_w: The bulk modulus of Waste.
- K_{hom}: The homogenized bulk modulus.
- v_c: The Poisson's ratio of Concrete.
- v_w : The Poisson's ratio of Waste.
- v_{hom}: The homogenized Poisson's ratio.
- V_c: The volume fractions of Concrete.
- V_w: The volume fractions of Waste.



http://www.doi.org/10.62341/AKBM2379

- α_{hom} : The homogeneous thermal conductivity.
- α_c : The thermal expansion coefficient of Concrete.
- α_w: The thermal expansion coefficient of Waste.
- γ_{hom} : The homogeneous thermal conductivity.
- γ_c : The thermal conductivity of Concrete.
- γ_w : The thermal conductivity of Waste.

$$E_{hom} = \frac{9K_{hom}G_{hom}}{3K_{hom} + G_{hom}};$$

$$G_{hom} = G_c + \frac{V_wG_c(G_w - G_c)}{G_c + \beta_1(1 - V_w)(G_w - G_c)};$$

$$K_{hom} = K_c + \frac{V_wK_c(K_w - K_c)}{K_c + \beta_2(1 - V_w)(K_w - K_c)}$$
(1)

Where:

$$\beta_1 = \frac{2(4 - 5V_c)}{15(4 - 5V_c)}; \beta_2 = 3 - 5\beta_1 \tag{2}$$

It's noted that; β_1 and β_2 represent the correction coefficients for spherical inclusions (reinforcement by waste) in a metal matrix (concrete) [15-16-17].

$$K_{c} = \frac{E_{c}}{3(1 - 2\nu_{c})};$$

$$K_{w} = \frac{E_{w}}{3(1 - 2\nu_{w})};$$

$$G_{s} = \frac{E_{s}}{2(1 + \nu_{s})};$$

$$G_{w} = \frac{E_{w}}{2(1 + \nu_{w})}$$
(3)

$$v_{\text{hom}} = \frac{3K_{\text{hom}} - 2G_{\text{hom}}}{6K_{\text{hom}} + 2G_{\text{hom}}} \tag{4}$$

$$V_{Concrete+Waste} = V_c + V_w = 1 (5)$$

$$\alpha_{\text{hom}} = \alpha_c - \frac{\lambda_w (\lambda_w (\lambda_w - (V_w \lambda_w + V_c \lambda_c))(\alpha_w - \alpha_c)}{(V_w \lambda_w + V_c \lambda_c)(\lambda_w - \lambda_c)}$$

$$\lambda_{\text{hom}} = \lambda_c + \frac{V_w \lambda_w (\lambda_w - \lambda_c)}{\lambda_c + \beta_1 (1 - V_w)(\lambda_w - \lambda_c)}$$
(6)



2. Thermo-mechanical bending model

The displacements are rewetting:

$$u(x,z) = u_0(x) - z \frac{\partial w_b}{\partial x} - f(z) \frac{\partial w_s}{\partial x}; v(x,z) = 0$$

$$w(x,z) = w_{b(x)} + w_{s(x)}$$
(7)

Function of shear deformation:

$$f(z) = \frac{4z^3}{3h^2} + \frac{7z^5}{13h^4} + \frac{9z^5}{25h^6} + \frac{11z^7}{35h^8} \qquad ; g = \left(1 - \frac{\partial f}{\partial z}\right)$$
 (8)

Displacements and distortions:

$$\varepsilon_{xx} = \frac{\partial u}{\partial x} = \frac{\partial u_0}{\partial x} - z \frac{\partial^2 w_b}{\partial x^2} - f(z) \frac{\partial^2 w_s}{\partial x^2}$$
(9)

$$\gamma_{xz} = \frac{\partial u}{\partial z} + \frac{\partial w}{\partial x} = g \frac{\partial w_s}{\partial x} \tag{10}$$

virtual work principal:

$$\int_{V} (\delta U + \delta V) = 0 \tag{11}$$

Substituting the constraints into equation number (11):

$$\delta U = \int_{0}^{L} \int_{A} \left[\sigma_{xx} + (\varepsilon_{xx} - \alpha_{\text{hom}} \Delta T) + \tau_{xz} \gamma_{xz} \right] dx dA$$
 (12)

Knowing that the constraint is a force factor on the surfaces, then:

$$\delta U = \int_{0}^{t} \left\{ N_{xx} \frac{\partial \delta u_{0}}{\partial x} - M_{b} \frac{\partial^{2} \delta w_{b}}{\partial x^{2}} - M_{s} \frac{\partial^{2} \delta w_{s}}{\partial x^{2}} - N_{xx}^{T} \alpha_{\text{hom}} \Delta T + Q_{xz} \frac{\partial \delta w_{s}}{\partial x} \right\} dx$$
 (13)

When:

$$\left(N_{xx}^{T}, M_{b}, M_{s}\right) = \int_{A} \sigma_{xx} \left(1, z, f\left(z\right)\right) dA \tag{14}$$

And:

$$Q_{xz} = \int_{A} g(z) \tau_{xz} dA \tag{15}$$

The external forces are designated as follows in equation number (16):

$$\delta V = -\int_0^l q \left(\delta w_b + \delta w_s \right) dx \tag{16}$$



By coupling equations (12) to (16) into equation (11), the equilibrium equations are written in the following form:

$$\delta u_0 : \frac{\partial N_{xx}}{\partial x} = 0$$

$$\delta w_b : -\frac{\partial^2 M_b}{\partial x^2} + q = 0$$

$$\delta w_s : -\frac{\partial^2 M_s}{\partial x^2} + \frac{\partial Q_{xx}}{\partial x} + q = 0$$
(17)

The normal and tangential stresses are defined as follows:

$$\begin{cases}
\sigma_{xx} \\
\tau_{xz}
\end{cases} = \begin{cases}
Q_{11} & 0 \\
0 & Q_{55}
\end{cases} \begin{cases}
\varepsilon_{xx} - \alpha_{\text{hom}} \Delta T \\
\gamma_{xz}
\end{cases}$$
(18)

When:

$$Q_{11} = E_{\text{hom}}, \quad Q_{55} = \frac{E_{\text{hom}}}{2(1 + v_{\text{hom}})}$$
 (19)

Replacing in (14):

$$N_{xx} = A \frac{\partial u_0}{\partial x} - B_s \frac{\partial^2 w_b}{\partial x^2} - D_s \frac{\partial^2 w_s}{\partial x^2} - N_{xx}^T$$

$$\boldsymbol{M}_{b} = \boldsymbol{B} \frac{\partial u_{0}}{\partial x} - \boldsymbol{D} \frac{\partial^{2} w_{b}}{\partial x^{2}} - \boldsymbol{D}_{s} \frac{\partial^{2} w_{s}}{\partial x^{2}} - \boldsymbol{M}_{b}^{T}$$

$$M_{s} = B_{s} \frac{\partial u_{0}}{\partial x} - D_{s} \frac{\partial^{2} w_{b}}{\partial x^{2}} - H_{s} \frac{\partial^{2} w_{s}}{\partial x^{2}} - M_{s}^{T}$$

$$(20)$$

Noted that:

$$Q_{xz} = A_s \frac{\partial w_s}{\partial x} \tag{21}$$

Where:

$$\left(N_{xx}^{T}, M_{b}^{T}, M_{s}^{T}\right) = Q_{11}\alpha_{\text{hom}}\Delta T \int_{A} \left(1, z, f(z)\right) dA$$

$$(A, B, B_s, D) = Q_{11} \int_A (1, z, f(z), z^2) dA$$

$$(D_s, H_s) = Q_{11} \int_A \left(f(z), f(z)^2 \right) dA$$
(22)

When:

$$A_{s} = \int_{A} Q_{55} g\left(z\right)^{2} dA \tag{23}$$



In which the last equilibrium equations written:

$$A\frac{\partial^2 u_0}{\partial x^2} - B\frac{\partial^3 w_b}{\partial x^3} - B_s \frac{\partial^3 w_s}{\partial x^3} = P_1$$

$$B\frac{\partial^2 u_0}{\partial x^2} - D\frac{\partial^3 w_b}{\partial x^3} - D_s \frac{\partial^3 w_s}{\partial x^3} = P_2$$

$$B_{s} \frac{\partial^{2} u_{0}}{\partial x^{2}} - D_{s} \frac{\partial^{3} w_{b}}{\partial x^{3}} - H_{s} \frac{\partial^{3} w_{s}}{\partial x^{3}} + A_{s} \frac{\partial^{2} w_{s}}{\partial x^{2}} = P_{3}$$

$$P_{1} = \frac{\partial N_{xx}^{T}}{\partial x}, P_{2} = \frac{\partial^{2} M_{b}^{T}}{\partial x^{2}}, P_{3} = \frac{\partial^{2} M_{s}^{T}}{\partial x^{2}} - q$$
(24)

Navier's solutions are written:

$$u = \sum_{n=1}^{\infty} U_n \cos(\lambda x) \quad w_b = \sum_{n=1}^{\infty} W_{bn} \sin(\lambda x)$$

$$W_s = \sum_{n=1}^{\infty} W_{sn} \sin(\lambda x) \lambda = \frac{n\pi}{L}, \quad (U_n, W_{bn}, W_{sn})$$
 (25)

The loads:

$$q(x) = \sum_{n=1}^{\infty} Q_n \sin(\lambda x)$$

General load:

$$Q_n = \frac{2}{L} \int_0^L q(x) \sin(\lambda x) dx \tag{26}$$

For sinusoidal load:

$$Q_n = q_0 \quad (n=1) \tag{27}$$

For uniform load:

$$Q_n = \frac{4q_0}{n\pi} \quad (n = 1, 3, 5, ...)$$
 (28)

Thermal load:

$$\begin{cases}
T_1 \\
T_2 \\
T_3
\end{cases} = \begin{cases}
t_1 \\
t_2 \\
t_3
\end{cases} \sin(\lambda x) \tag{29}$$

In which:



$$\Delta T(x,z) = T_1(x) + zT_2(x) + \psi(z)T_3(x)$$
(30)

T1: Linear distribution with thickness z.

T2: non-linar distribution with thickness z.

T3: Coupled T1+T2.

Stiffness matrix is:

$$\begin{bmatrix} S_{11} & S_{12} & S_{13} \\ S_{21} & S_{22} & S_{23} \\ S_{31} & S_{32} & S_{33} \end{bmatrix} \begin{Bmatrix} U_n \\ W_{bn} \\ W_{sn} \end{Bmatrix} = \begin{Bmatrix} P_1 \\ P_2 \\ P_3 \end{Bmatrix} S_{22} = -D\lambda^4,$$

$$S_{23} = -D_s\lambda^4,$$

$$S_{23} = -D_s\lambda^4,$$

$$S_{33} = -(H_s\lambda^4 + A_s\lambda^2)$$

$$(31)$$

Where, forces are written:

$$P_{1} = \lambda \left[A^{T} t_{1} + B^{aT} t_{2} + B_{s}^{aT} t_{2} \right]; P_{2} = -\lambda^{2} \left[B^{bT} t_{1} + D^{T} t_{2} + D_{s}^{bT} t_{3} \right] - q$$

$$P_{3} = -\lambda^{2} \left[B_{s}^{cT} t_{1} + D_{s}^{cT} t_{2} + H^{T} t_{3} \right] - q;$$

$$\left(A^{T}, B^{aT}, B_{s}^{aT} \right) = Q_{11} \int_{A} \alpha \{1, z, \psi(z)\} dA$$
(32)

Noted that:

$$(B^{bT}, D^{T}, D_{s}^{T}) = Q_{11} \int_{A} \alpha \{z, z^{2}, z \psi(z)\} dA$$

$$(B_{s}^{cT}, D_{s}^{cT}, H^{T}) = Q_{11} \int_{A} \alpha \{f(z), z f(z), f(z) \psi(z)\} dA$$
(33)

The dimensionless parameters are written as follows to simplify calculations and the reading of the results.

$$\overline{u} = 100 \frac{E_m h^3}{q_0 l^4} u \left(0, \frac{h}{2}\right) \quad \overline{w} = 100 \frac{E_m h^3}{q_0 L^4} w \left(\frac{L}{2}, 0\right)$$

$$\overline{\sigma_x} = \frac{h^3}{q_0 l} \sigma_x \left(\frac{L}{2}, \frac{h}{2}\right) \qquad \overline{\tau_{xz}} = \frac{h}{q_0 l} \tau_{xz} \left(0, 0\right)$$
(34)

Boundary conditions:

At:
$$x = 0, x = L$$

$$U = W = M_x^b = M_x^s = 0$$



3. Validation of the Mori-Tanaka homogenization model

The material parameters (tungsten steel) from articles [11] and [12] are presented in Table 1. Their comparison is then presented in Table 2.

Table 1: The material parameters (tungsten steel).

Materials	Young's Modulus [GPa]	Poisson's ratio
Steel	200	0.33
Tungsten	500	0.28

Table 2: The results of homogenization by Mori-Tanaka.

Properties	Young's Modulus		Poisson's ratio	
	[GPa]			
Materials	[11] and Present		[11] and	Present
	[12]		[12]	
Steel + 10% Tungsten	220.20	220.19	0.325	0.323
Steel + 20% Tungsten	240.33	240.31	0.320	0.316
Steel + 30% Tungsten	260.40	260.38	0.315	0.301

The results in Table 2 show that the current Mori-Tanaka method is in good agreement with the results from [11] and [12]. This validates our current homogenization program.

4. Validation of the thermo-mechanical model

Based on the article by S. M. Ghumarea and A. S. Sayyada [29], an isotropic material is modeled as a functionally graded material (FGM) for P=0.show table 3; when Ceramic [50]: E=380 GPa; v=0.3; α =7.4*10⁻⁶ °C⁻¹and Aluminium [50]: E=70 GPa; v=0.3; α =23*10⁻⁶ °C⁻¹.

Table 3: Validation of a thermomechanical program with an FGM material at P=0.

Theory	Conditions : $L/h = 10$; $T1 = 10$; $q_0 = 100$			
Parameters	\overline{u}	\overline{w}	$\overline{\sigma}_x$	$\overline{ au}_{\scriptscriptstyle xz}$
S.M and A.S [49]	0.44	2.8214	7.6973	0.4768
Present	0.4561	2.9628	7.7798	0.4831
Theory	Conditions:	L/h = 10;	T1 = 10; $T2 = 1$	$0; q_0 = 100$
Parameters	\overline{u}	\overline{w}	$\overline{\sigma}_x$	$\overline{ au}_{\scriptscriptstyle XZ}$
S.M and A.S [49]	0.5015	3.2265	9.8165	0.4768
Present	0.5162	3.3882	9.9217	0.4831



The results in Table 3 show a high degree of convergence, which allows us to conclude that the thermomechanical model used in this study is valid.

5. Results and discussion

Eco-concrete with waste Pottery

Using data from the articles by Benfrid et al. [4] and [9] to estimate the effective properties of eco-concrete reinforced with Pottery particles, Table 4 shows the properties used in this study, and Table 5 shows the properties of an eco-concrete reinforced successively with 10%, 20%, and 30% Pottery powder. Specifically, aluminosilicate waste Pottery powder is used in this study.

Table 4: The properties used in this study (Concrete and aluminosilicate waste Pottery powder).

Materials	Young's Modulus [GPa]	Poisson's ratio	Thermal expansion 10 ⁻⁶ °C ⁻¹
Concrete [4] and [9]	20	0.3	13.5
aluminosilicate waste Pottery powder [4] and [9]	81	0.16	4.6

Table 5: The properties of eco-concrete reinforced with aluminosilicate waste Pottery powder.

Materials	Young's Modulus [GPa]	Poisson's ratio	Thermal expansion 10 ⁻⁶ °C
Concrete + 0% aluminosilicate waste Pottery powder	20	0.300	13.500
Concrete + 10% aluminosilicate waste Pottery powder	26.087	0.269	9.651
Concrete + 20% aluminosilicate waste Pottery powder	32.117	0.246	7.878
Concrete + 30% aluminosilicate waste Pottery powder	38.130	0.228	6.899

It is noted from the asymptotic homogenization results presented in Table 5 that the Young's modulus increases each time the volume fraction of Pottery waste increases. Furthermore, the thermal expansion and Poisson's coefficient decrease.



Mechanical Bending

Table 6 presents the purely mechanical static bending for concrete reinforced with aluminosilicate waste Pottery powder, with parametric changes in geometry in terms of length-to-thickness ratio, where q_0 =100.

Table 6: Mechanical static bending for concrete reinforced with aluminosilicate waste Pottery powder

Conditions	$L/h = 10; T1 = 0; T2 = 0; q_0 = 100$				
Parameters	\overline{u}	\overline{w}	$\overline{\sigma}_x$	$\overline{ au_{_{X\!Z}}}$	
Concrete + 0% aluminosilicate waste Pottery powder	2.4750	16.0870	7.7775	0.6271	
Concrete + 10%aluminosilicate waste Pottery powder	1.8973	12.3265	5.9594	0.4807	
Concrete + 20% aluminosilicate waste Pottery powder	1.5409	10.0075	4.8382	0.3903	
Concrete + 30% aluminosilicate waste Pottery powder	1.2978	8.4263	4.0738	0.3288	
Theory	Condition	ns : L/h = 50;	T1 = 0; T2 = 0	; $q_0 = 100$	
Conditions	\overline{u}	\overline{w}	$\overline{\sigma}_x$	$\overline{ au_{_{_{XZ}}}}$	
Concrete + 0% aluminosilicate waste Pottery powder	0.4928	15.7013	38.7085	0.6275	
Concrete + 10% aluminosilicate waste Pottery powder	0.3778	12.0375	29.6768	0.4810	
Concrete + 20% aluminosilicate	0.3069	9.7771	24.1041	0.3907	



waste Pottery powder				
Concrete + 30% aluminosilicate waste Pottery powder	0.2585	8.2352	20.3026	0.3291

According to Table 6, it is noted that in mechanical bending, each time the concentration of aluminosilicate increases, the deflection and transverse displacements as well as the stresses decrease. This means that concrete reinforced with aluminosilicate provides perfect rigidity, which reduces the deflection. Furthermore, the deflection decreases for more slender beams, but the stress concentration becomes greater than that for short beams. Figure 1 shows the transverse displacements and deflections for different concentrations of aluminosilicate Pottery powder.

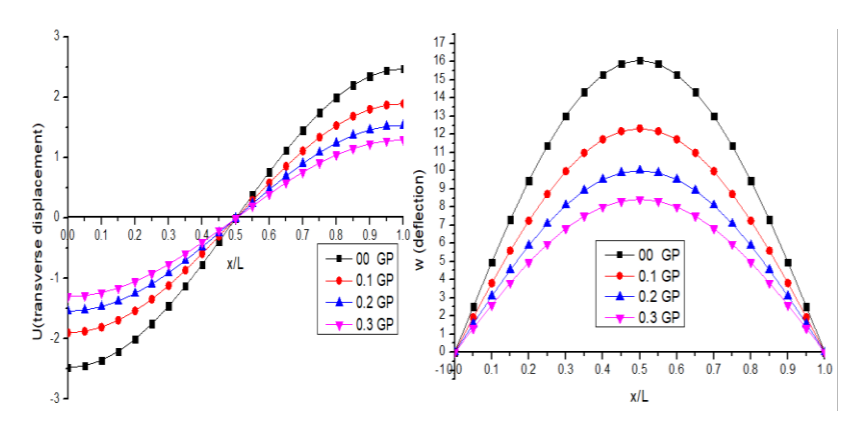


Figure 1: The curves of transverse displacements and deflection as a function of the concentration of Pottery powder.

According to the graph of transverse displacements, it is noted that all fractions give symmetrical curves. They start from negative values at the center of the beam, become zero, and then turn positive. As for the deflection, the curves start from zero and end at zero along the beam's length, with the maximum value at the center of the curves, which means that the static bending is correct. Furthermore, because the aluminosilicate powder gives good rigidity to the beams, it is noted that each time the volume fraction of the Pottery powder increases, the deflection decreases, which is a good positive



indicator for eco-concrete reinforced with aluminosilicate Pottery powder.

Thermo-mechanical Bending

In this section, a thermal bending study was performed with a fixed load of q_0 =100. In the first example, a condition of T_1 =10was added. Next, a second case with T_1 = T_2 =10 was considered for a parameter check. The results are presented in Table 7.

Table 7: Thermo-mechanical Bending for concrete reinforced with aluminosilicate waste Pottery powder

Conditions	L/h = 10;	$L/h = 10$; $T1 = 10$; $T2 = 0$; $q_0 = 100$				
Parameters	\overline{u}	\overline{w}	$\overline{\sigma}_{x}$	$\overline{ au_{_{XZ}}}$		
Concrete	2.4793	16.0954	7.7776	0.5502		
+ 0%						
aluminosilicate						
waste Pottery						
powder						
Concrete	1.9017	12.3351	7.7775	0.5244		
+ 10%						
aluminosilicate						
waste Pottery						
powder						
Concrete	1.5453	10.0159	7.7774	0.4984		
+ 20%						
aluminosilicate						
waste Pottery						
powder						
Concrete	1.3022	8.4347	7.7773	0.4719		
+ 30%						
aluminosilicate						
waste Pottery						
powder		10 51 50	10 10			
Conditions		=10;T1=T2=	:10 ;q ₀ =10	0		
Parameters	\overline{u}	\overline{w}	$\overline{\sigma}_x$	$\overline{ au_{xz}}$		
Concrete	2.4707	16.1001	7.3624	0.7041		
+ 0%						
aluminosilicate						
waste Pottery						
powder						
Concrete	1.8931	12.3398	7.2333	0.7299		
+ 10%						
aluminosilicate						
waste Pottery						
powder						



Concrete	1.5366	10.0206	7.1060	0.7560
+ 20%				
aluminosilicate				
waste Pottery				
powder				
Concrete	1.2935	8.4394	6.9794	0.7824
+ 30%				
aluminosilicate				
waste Pottery				
powder				

According to the results in Table 7, it is noted that in thermomechanical bending, each time the volume fraction increases, all the parameters decrease. In the case of a simultaneous application of T₁And T₂, the deflection and the concentrations of normal and tangential stresses also decrease. This decrease is due to the reduction in thermal expansion and the increase in rigidity. Figure 2 shows the influence of temperature on the deflection and transverse displacements of ordinary concrete beams and beams reinforced with 30% aluminosilicate Pottery powder under various thermal loads.

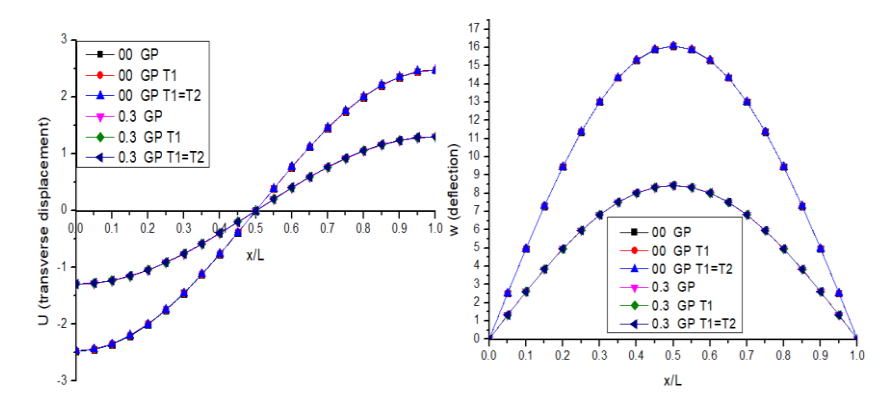


Figure 2 : Comparison of thermal bending between ordinary concrete and concrete reinforced with 30% Pottery powder.

The observation from reading the graphs illustrated in Figure 2 is that the Pottery powder gives good resistance to the concrete, even under the application of a thermal load or the influence of temperature, because the thermal expansion will be very slight.

6. Conclusion

In conclusion, we can extract five key points from this work. Firstly, the eco-concrete perfectly withstands mechanical behavior, and the aluminosilicate provides perfect rigidity to this new concrete.



http://www.doi.org/10.62341/mekh2627

Secondly, these concrete resists thermomechanical behavior, and the variation in external temperature doesn't influence its deflection or stresses. Thirdly, the eco-concrete reinforced with Pottery powder can be modeled using the Mori-Tanaka rule of biphasic homogenization. Fourthly, this eco-concrete will be useful from an environmental and ecological standpoint by reducing CO₂ emissions. Finally, the use of this eco-concrete offers an economic advantage because it can replace cement, and it promotes a recycling approach. The deflection decreases with the increase in pottery powder, and the optimal fraction is 30%, which yields the best results.

References

- [1] Boukhelf, F., Cherif, R., Trabelsi, A., Belarbi, R., & Bouiadjra, M. B. (2021). On the hygrothermal behavior of concrete containing glass powder and silica fume. Journal of Cleaner Production, 318, 128647.
- [2] Harrat, Z. R., et al. (2021). On the static behavior of nano SiO2-based concrete beams resting on an elastic foundation. Computational Concrete, 27(6), 575.
- [3] Chatbi, M., et al. (2022). Bending analysis of nano-SiO2 reinforced concrete slabs resting on elastic foundation. Structural Engineering and Mechanics, 84(5), 685–697.
- [4] Benfrid, A., et al. (2023). Thermomechanical analysis of glass powder-based eco-concrete panels: Limitations and performance evaluation. Periodica Polytechnica Civil Engineering, 67(4), 1284–1297.
- [5] Elhennani, S. D., et al. (2023). Buckling and free vibration analyses of various nanoparticle reinforced concrete beams resting on multi-parameter elastic foundations. Materials, 16(17), 5865.
- [6] Kecir, A., et al. (2024). Enhancing the mechanical performance of concrete slabs through the incorporation of nano-sized iron oxide particles (Fe2O3): Non-local bending analysis. Periodica Polytechnica Civil Engineering, 68(3), 842–858.



- [7] Chatbi, M., et al. (2023). Nano-clay platelet integration for enhanced bending performance of concrete beams resting on elastic foundation: An analytical investigation. Materials, 16(14), 5040.
- [8] Harrat, Z. R., et al. (2023). Modeling the thermoelastic bending of ferric oxide (Fe2O3) nanoparticles-enhanced RC slabs. Materials, 16(8), 3043.
- [9] Benfrid, A., et al. (2025). Selective integration of waste-derived glass nanopowders in structural wall concrete: Improving thermal efficiency and elasto-mechanical properties for sustainable construction. Periodica Polytechnica Civil Engineering, 69(3), 954–965.
- [10] Benfrid, A., & Bouiadjra, M. B. (2025). A new approach for studying plaster beam bending based on DISS Algerian (nanoshort-bio-fibres). Modern Journal of Health and Applied Sciences, 2(1), 43–58.
- [11] Benbakhti, A., et al. (2024). An analytical analysis of the hydrostatic bending to design a wastewater treatment plant by a new advanced composite material. Journal of Composite & Advanced Materials/Revue des Composites et des Matériaux Avancés, 34(2).
- [12] Lakhder, M., et al. (2025). The mechanical bending behavior of a new metal alloy nano-reinforced plate incorporating tungsten nanoparticles. NIPES-Journal of Science and Technology Research, 7(3), 423–440.
- [13] Wang, X., Sun, K., Shao, J., & Ma, J. (2023). Fracture properties of graded basalt fiber reinforced concrete: Experimental study and Mori-Tanaka method application. Construction and Building Materials, 398, 132510.
- [14] Zheng, H., Zhang, L., Dong, Q., & Sun, G. (2024). Prediction of the effective diffusion coefficient on sulfate ions in heterogeneous concrete based on Mori-Tanaka scheme. Construction and Building Materials, 449, 138326.



- [15] Yang, C.-C., & Huang, R. (1996). Double inclusion model for approximate elastic moduli of concrete material. Cement and Concrete Research, 26(1), 83–91.
- [16] Pan, J., & Bian, L. (2019). A re-formulation of the Mori–Tanaka method for predicting material properties of fiber-reinforced polymers/composites. Colloid and Polymer Science, 297(4), 529–543.
- [17] Park, I., Moon, J., Bae, S., Oh, J. E., & Yoon, S. (2020). Application of micro-CT to Mori-Tanaka method for non-randomly oriented pores in air-entrained cement pastes. Construction and Building Materials, 255, 119342.
- [18] Liu, L., & Huang, Z. (2014). A note on Mori-Tanaka's method. Acta Mechanica Solida Sinica, 27(3), 234–244.
- [19] Miled, K., & Limam, O. (2016). Effective thermal conductivity of foam concretes: Homogenization schemes vs experimental data and FEM simulations. Mechanics Research Communications, 76, 96–100.
- [20] Wang, H. W., Zhou, H. W., Peng, R. D., & Mishnaevsky Jr., L. (2011). Nanoreinforced polymer composites: 3D FEM modeling with effective interface concept. Composites Science and Technology, 71(7), 980–988.
- [21] Ghumare, S. M., & Sayyad, A. S. (2019). Nonlinear hygrothermo-mechanical analysis of functionally graded plates using a fifth-order plate theory. Arabian Journal for Science and Engineering, 44(10), 8727–8745.
- [22] Boulahbal, Y., et al. (2025). On the bending behavior of nonhomogeneous nanoscale beams under nonlinear hygrothermo-mechanical loading. Acta Mechanica, 1–21.
- [23] Ertenli, M. F., & Esen, I. (2025). Thermo-mechanical buckling response of functionally graded sandwich dome structures. Archive of Applied Mechanics, 95(4), 82.
- [24] Sayyad, A. S., Shinde, B. M., & Kant, T. (2023). Hygrothermo-mechanical analysis of sandwich shallow shells



- considering the effects of transverse normal strain. Journal of Thermal Stresses, 46(7), 639–671.
- [25] Meski, K., Mamen, B., & Menasria, A. (2024). Analytical solutions for the thermo-mechanical bending of FG beams using a higher-order shear deformation theory (HSDT). MATEC Web of Conferences, 394, 03004.
- [26] Mori, T., & Tanaka, K. (1973). Average stress in matrix and average elastic energy of materials with misfitting inclusions. Acta Metallurgica, 21(5), 571–574.
- [27] Chardonnet, J. R., Amaro, A. de C., Léon, J. C., & Cani, M. P. (2009). Hand Navigator: Prototypages de périphériques d'interaction pour le contrôle d'une main virtuelle. In 4ème Journées de l'Association Française de Réalité Virtuelle.
- [28] Temam, R. (2024). Navier–Stokes Equations: Theory and Numerical Analysis (Vol. 343). American Mathematical Society.
- [29] Murawski, K. (2021). Experimental comparison of the known hypotheses of lateral buckling for semi-slender pinned columns. International Journal of Structural Glass and Advanced Materials Research, 5(1), 82–114.
- [30] Murawski, K. (2018). Technical stability of very slender orthotropic panels with thin walls. Journal of Structural Stability, 5(1), 134–194.
- [31] Murawski, K. (2021). Technical buckling, stress and strain simplified analysis of semi-slender thin-walled cylindrical pinned column. International Journal of Structural Glass and Advanced Materials Research, 5(1), 134–194.
- [32] Ike, C. (2025). Ritz variational method for free harmonic vibration solutions of slender beams on two-parameter elastic foundations. Nigerian Journal of Technology, 44(2), 193–201.
- [33] Ike, C. (2024). Stodola-Vianelo iteration method for solving the natural harmonic transverse vibration problems of Euler-Bernoulli beams on Winkler foundations. Iraqi Journal of Civil Engineering, 18(2), 73–87.



- [34] Mladenov, K. A. (1992). On the critical and post-critical behavior of plane frames. Journal of Constructional Steel Research, 21(1–3), 97–113.
- [35] Doicheva, A. (2022). Finite element method for the analysis of eccentrically connected continuous beams. The Eurasia Proceedings of Science, Technology, Engineering & Mathematics (EPSTEM), 18, 37–45.
- [36] Ahmed, B., Hafida, D., Djihad, R., & Abdelmoutalib, B. (2025). Bending performance of concrete beams incorporating granite waste. Veredas do Direito, 22(2), e3155–e3155.
- [37] Yerkrou, A., Benfrid, A., Krour, B., & Bouiadjra, M. B. (2025). A programming model for analyzing the mechanical and thermal buckling behavior of eco-concrete panels incorporating recycled waste materials (glass and red bricks). Veredas do Direito, 22(2), e3117–e3117.
- [38] Lakhder, M., Benfrid, A., Bouiadjra, M. B., Chatbi, M., Harrat, Z. R., & Benbakhti, A. (2025). Mechanical bending behavior of a new nano-reinforced metallic alloy plate incorporating tungsten nanoparticles. NIPES-Journal of Science and Technology Research, 7(3), 423–440.
- [39] Peker, F. Ü., Yuzbasi, J., Işık, E., Büyüksaraç, A., & Avcil, F. (2025, October). Damage evaluation, regional ground motion analysis, and seismic performance analysis of a 14-story high-rise dual-system building after the 2023 Kahramanmaraş earthquakes. In Structures (Vol. 80, p. 109897). Elsevier.
- [40] Aras, F., Doğan, T. P., Öztürk, M., Tün, M., Işık, E., & Arslan, M. H. (2025). Assessment of the damage caused by the 6 February 2023 earthquakes on old and new dated reinforced concrete buildings in Elbistan, Turkey. Advances in Structural Engineering, 13694332251375194.
- [41] Işık, E., Radu, D., Harirchian, E., Avcil, F., Arkan, E., Büyüksaraç, A., & Hadzima-Nyarko, M. (2025). Failures in reinforced-concrete columns and proposals for reinforcement solutions: Insights from the 2023 Kahramanmaraş earthquakes. Buildings, 15(9), 1535.



- [42] Bahadır, F. C., & Turan, F. (2024). Free vibration responses of orthotropic laminated cylindrical panels with non-uniform porosity distributions using higher-order shear deformation theory. Mechanical Design of Structures and Machines, 52(12), 9975–10005.
- [43] Murawski, K. (2023). Technical analysis of lateral buckling, stresses, and simplified deformations with Aall, Jzall, Epl=Ec of a semi-slender thin-walled cylindrical pinned column in St35 steel. Stability Structural Journal of Critical Engineering, 1–67.
- [44] Tien, D. N., Tung, N. X., & Lam, N. N. (2024). Analytical solution for the bending of steel-concrete composite plates considering shear deformation effects. Engineering, Technology & Applied Science Research, 14(5), 16090–16094.
- [45] Anh, B. T., Hiep, N. T., & Van Lap, N. (2024). Finite element analysis of free vibrations of rigid pavements on non-uniform elastic foundations. Engineering, Technology & Applied Science Research, 14(1), 12452–12456.
- [46] Turan, F., Basoglu, M. F., & Hoang, V. N. V. (2025). Lateral-torsional stability of thin-walled orthotropic porous I-beams with non-uniform porosity distributions subjected to uniformly distributed load. Acta Mechanica, 236(1), 153–171.
- [47] Peng, L. X., Chen, S. Y., Chen, W., & He, X. C. (2023). A moving Kriging interpolation meshless method for bending and free vibration analysis of stiffened FGM plates in thermal environments. International Journal of Computational Methods, 20(10), 2350015.
- [48] Ghumare, S. M., & Sayyad, A. S. (2020). Nonlinear hygrothermo-mechanical analysis of functionally graded plates using a fifth-order plate theory. Applied Computational Mechanics, 14(1).
- [49] Lezgy-Nazargah, M. (2015). Fully coupled thermo-mechanical analysis of bi-directional FGM beams using NURBS isogeometric finite element approach. Aerospace Science and Technology, 45, 154–164.



http://www.doi.org/10.62341/mekh2627

[50] Mori, T., & Tanaka, K. (1973). Average stress in matrix and average elastic energy of materials with misfitting inclusions. Acta Metallurgica, 21(5), 571–574.